journal

J. Am. Ceram. Soc., 90 [9] 2966–2973 (2007)
DOI: 10.1111/j.1551-2916.2007.01832.x

Electrodeposition of *p*-Type CuSCN Thin Films by a New Aqueous Electrolyte With Triethanolamine Chelation

Yong Ni, Zhengguo Jin,† and Yanan Fu

Key Laboratory for Advanced Ceramics and Machining Technology of Ministry of Education, School of Materials Science and Engineering, Tianjin University, Tianjin 300072, China

A stable aqueous electrolyte solution containing Cu^{2+} and SCN^- was prepared by adding triethanolamine (TEA, $N(CH_2CH_2OH)_3$) to chelate with Cu(II) cations. The electrolyte solutions were basic, with pH values in the range of 8.5–9, and could be used in the electrodeposition of CuSCN as a hole-conducting layer on a ZnO substrate and as an electron-conducting layer for nanocrystal photovoltaic cells because it could prevent the ZnO layer from acidic etching. CuSCN films were potentiostatically deposited on indium tin oxide glass substrates through the aqueous solutions, and the deposition potential for the sole CuSCN phase layer was determined by a linear sweep voltammetry measurement. The influence of applied potentials, electrolyte components, and deposition temperatures on the stoichiometry, phase, and particle morphology of the CuSCN films was investigated by X-ray photoelectron spectra, X-ray diffraction, and a field-emission scanning electron microscope. The results showed that the morphology of the dense CuSCN films was trigonal pyramid and the stoichiometric portions of SCN/Cu were excess of SCN. The current–voltage (*I–V*) characteristic of the junction between electrodeposited CuSCN and ZnO nanostructured layer displayed *p*-type semiconductor characteristics of CuSCN. The transmittance measurements detected high transmittance ($\geq$ 87%) in the visible wavelength range, and the direct transition band gap calculated was 3.88 eV.

I. Introduction

NANOCRYSTAL photovoltaic cells (NPC), such as dye-sensitized solar cells (DSSCs)[1–7] and extremely thin absorber (ETA) solar cells,[8–14] have been receiving increasing attention because of their advantages of low cost and high efficiency, which presage commercial applications.[1] Generally, NPC cells mainly consist of a nano- or microstructured layer of an *n*-type wide-band-gap semiconductor, a sensitization layer, and an electrolyte layer as a hole-conducting layer. The *n*-type semiconductor serves as electron conductors, and in DSSCs, it also serves as a supporting layer for the adsorbed dyes. The most widely used *n*-type semiconductors are porous TiO_2[1,2,15] and ZnO nanowire films.[8,11,13,14] The nano- or microstructured character of these films results in great surface area enlargement. To make use of the high internal surface of the *n*-type layer, the pores must be filled completely with absorbers and hole conductors. Liquid electrolytes are well suited to this role. However, problems associated with the liquid electrolytes, such as dye desorption, solvent evaporation and degradation, seal imperfections, and reaction of the sealant with electrolyte,[16,17] have encouraged studies on solid-state or quasi-solid-state hole conductors, such as *p*-type semiconductors, ionic liquid electrolytes, and polymer electrolytes.[18–22] A *p*-type semiconductor is a good candidate for a solid-state electrolyte, which has some advantages in improving the long-term durability and stability of NPC cells. There are some wide band gap materials, such as CuI,[16,20] $CuAlO_2$,[23] NiO,[24] and CuSCN,[4,5,25] which can meet the requirements for the *p*-type layer of NPC solar cells. Among these, CuSCN is thought to be the most promising for its stability and possibility in filling the pores of the highly structured *n*-type layer by solution deposition,[8,26] CBD,[27] SILAR,[27] and electrodeposition,[5,19,25] in which electrodeposition is a feasible method for coating the insides of complex shapes.

Recently, there have been some studies on ZnO used as an *n*-type anode for NPC solar cells. Compared with the TiO_2 anode, ZnO has a higher electron mobility (200 $cm^2 \cdot (V \cdot s)^{-1}$)[28] than anatase TiO_2 (10 $cm^2 \cdot (v \cdot s)^{-1}$).[29] O'Regan *et al.*[5] had studied the cell structure and performance of ZnO/dye/CuSCN devices and achieved higher quantum efficiency and energy efficiency than TiO_2/dye/CuSCN devices. Lévy-Clément *et al.*[8] succeeded in achieving an innovative composite nanostructure ZnO/CdSe/CuSCN, based on free-standing ZnO nanowire arrays. In these studies, preparation of CuSCN layers by electrodeposition using organic solvents had been reported.[5,19,25] However, organic solvents had a few technical disadvantages in the electrodeposition of the *p*-type semiconductors applied in NPC cells. Typically, use of organic solvents led to poor conductivity of the deposition solution, dye desorption on the *n*-type layer, and poor contact with the sensitization layer.[19,30] To avoid these technical disadvantages, electrodeposition of CuSCN films in an aqueous solution should be a better choice because there are many advantages for electrodeposition in an aqueous solution, such as high conductivity, strong dissolvability to solutes, high deposition efficiency, and especially in preventing desorption of dyes. Nevertheless, it is difficult to electrodeposit CuSCN by an aqueous solution because of the poor stability of Cu(II) cations and SCN anions in water.[25] Wu *et al.*[31] had succeeded in preparing a stable aqueous electrolyte solution using ethylenediamine tetraacetic acid (EDTA) disodium salt as the chelating agent for Cu(II) cations, and obtaining dense CuSCN films by electrodeposition in acidic electrolyte solutions with a pH value of about 2. However, the pH value of the electrolyte is so low that ZnO as a bottom substrate for NPC devices is easy to be etched. Hence, a neutral or weak basic aqueous electrolyte solution is required to deposit CuSCN films on ZnO substrates for NPC solar cells.

In the present paper, the research work is mainly focused on the electrodeposition and characterization of CuSCN films through new triethanolamine (TEA, $N(CH_2CH_2OH)_3$)-chelated aqueous electrolytes with weak basic. Based on the electrodeposition feature determined by linear sweep voltammetry (LSV) measurement, the influence of the applied potentials, electrolyte component, and deposition temperature on the stoichiometric proportion and morphology of the as-prepared CuSCN films is primarily investigated, and its optical property is characterized.

M. P. Paranthaman—contributing editor

Manuscript No. 22779. Received February 7, 2007; approved April 24, 2007.
This work was financially supported by Key Basic Research of TSTC.
†Author to whom correspondence should be addressed. e-mail: zhgjin@tju.edu.cn

II. Experimental Procedure

Cupric sulfate pentahydrate ($CuSO_4 \cdot 5H_2O$) and potassium thiocyanate (KSCN) as precursors and TEA as a chelating reagent for Cu(II) cations were used. They were all analytical-grade reagents. Aqueous electrolytes were firstly prepared by mixing cupric sulfate solutions with TEA solutions at the molar ratio $[Cu^{2+}]$:[TEA] = 1:10 and the concentration of Cu^{2+} was maintained at 0.01*M*. Then, KSCN solutions with the concentration range of 0.005–0.1*M* were added to the $CuSO_4$/TEA complex solutions under stirring for 1 h and then stored for 24 h before being electrodeposited. The pH value of the final solution was 8.5–9, varying with the concentration of KSCN.

The electrodeposition was carried out in a normal three-electrode cell. The electrochemical measurement was performed on a potentiostat/galvanostat (TD3691, Tianjin Zhonghuan Electronic Instrument Company, Tianjin, China). Indium tin oxide (ITO)-coated glass (10 Ω/cm) was used as a working electrode, a large area Pt foil as a counter electrode, and an $Ag/AgCl_{sat}$ as a reference electrode. Before deposition, ITO substrates were cleaned ultrasonically in acetone, 0.1 mol/L NaOH, and deioned water, respectively. A CuSCN film was electrodeposited potentiostatically ranging from −200 to −500 mV versus $Ag/AgCl_{sat}$ at varied temperatures. The potentials mentioned below were all in volts versus the $Ag/AgCl_{sat}$ reference electrode. Typically, the lower 1 cm of a 1 cm × 2.5 cm substrate was vertically placed in electrolyte solutions and about 2 cm from the counter electrode. The voltage was applied after stabilization for 30 s and the electrolyte was not stirred. The electrodeposition time was 30 min for all samples.

The phase composition of as-prepared films was analyzed by X-ray diffraction (XRD) on a Rigaku D/Max-2500 X-ray diffractometer (Tokyo, Japan) with Cu*K*α radiation (λ = 1.541 Å). The microstructures of the films were observed by a JSM-6700 field-emission scanning electron microscope (FESEM) from JEOL (Tokyo, Japan). X-ray photoelectron spectra (XPS) of films were obtained on an Esca Multiplex Philips-1600 X-ray photoelectron spectrometer (Eindhoven, the Netherlands). The current–voltage (*I–V*) characteristic was determined on the potentiostat/galvanostat (TD3691). The transmittance spectrum of the film was recorded on a Beckman DU-8B (Fullerton, CA) ultraviolet–visible (UV–Vis) absorption spectrometer.

III. Results and Discussion

LSV was used to investigate the role of TEA in the electrolyte solution and survey CuSCN electrodeposition from the prepared solutions. The linear sweep voltammetric curves ①–④ in Fig. 1 represent the electrolyte solutions consisting of 0.01*M* $CuSO_4$+0.10*M* TEA+0.05*M* KSCN, 0.01*M* $CuSO_4$+0.10*M* TEA, 0.01*M* $CuSO_4$, and 0.05*M* KSCN, respectively. On comparing curve ② with curve ③, the cathodic threshold potential for the reduction of Cu^{2+} to Cu^{+} ions in a $CuSO_4$+TEA solution is about −200 mV, while about 50 mV for the $CuSO_4$ solution, and at the same time, curve ② has a less cathode reaction current density, indicating that Cu(II)–TEA complexes were formed in the $CuSO_4$+TEA solution and resulted in a shift of the reduction potential to a more negative range as well as a decrease in the cathode reaction current density. Hence, it can be concluded that the stable mechanism of the Cu(II) cations and SCN anions in an aqueous solution is the formation of Cu(II)–TEA complexes, which is a feasible method to achieve the electrodeposition of CuSCN in a neutral aqueous electrolyte solution. For curve ①, the current density began to increase at the potential of −200 mV, displaying the cathodic threshold for electrodeposition of CuSCN, and subsequently increased gradually with potential in this diffuse-controlled region.[32] In the potential range of −550 to −900 mV, the current density becomes gently, showing that the reaction reached a saturated state accompanied by a minor co-deposition of copper.[33] Beyond −900 mV, the current density ascended again, showing that dominant deposition changed from the formation of CuSCN to copper reduction. For the curve of ④, the cathode reaction began at an applied potential of about −1350 mV, which could be attributed to the reduction of H^+ in the aqueous solution to form H_2. The high cathodic threshold potential indicates that KSCN did not undergo any reaction in the CuSCN deposition process and just supplied SCN anions. Hence, the growth process of CuSCN from the TEA-chelated aqueous solution could be suggested to be such that the cupric ions of the Cu(II)–TEA complexes that stably existed in the electrolyte solutions were first reduced to cuprous ions ($Cu^{2+}+e^- \rightarrow Cu^+$), and then CuSCN was formed by the reaction between a cuprous ion and a thiocyanate ion ($Cu^+ + SCN^- \rightarrow CuSCN$). Such a sole deposition could take place in a potential window between −200 and −550 mV. After this, Cu co-deposition would occur. Hence, it was concluded that the appropriate deposition potentials in the sole deposition of CuSCN in the TEA-chelated aqueous solution could be selected to be in the potential range of −200 to −550 mV.

To further study the influence of the applied potentials in the range of −200 to −550 mV on the nucleation and growth of electrodeposited CuSCN films, chronoamperometry measurements based on the current transient recording during the electrodeposition process were performed on bare ITO electrodes in the electrolyte solutions consisting of 0.01*M* Cu^{2+} and 0.05*M* SCN^- at room temperature. All measurements were carried out by stepping the potential of the working electrode from an open-circuit potential of 150 mV to potentials of −200, −300, −400,

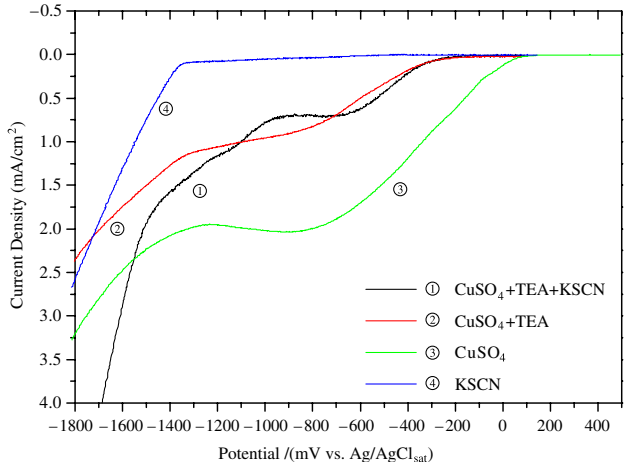

Fig. 1. Linear sweep voltammetric curves of the electrolyte solutions consisting of 0.01*M* $CuSO_4$+0.10*M* TEA+0.05*M* KSCN, 0.01*M* $CuSO_4$+0.10*M* TEA, 0.01*M* $CuSO_4$, and 0.05*M* KSCN, in the range of 500 to −1800 mV on the indium tin oxide electrode at a rate of 50 mV/s. TEA, triethanolamine; KSCN, potassium thiocyanate.

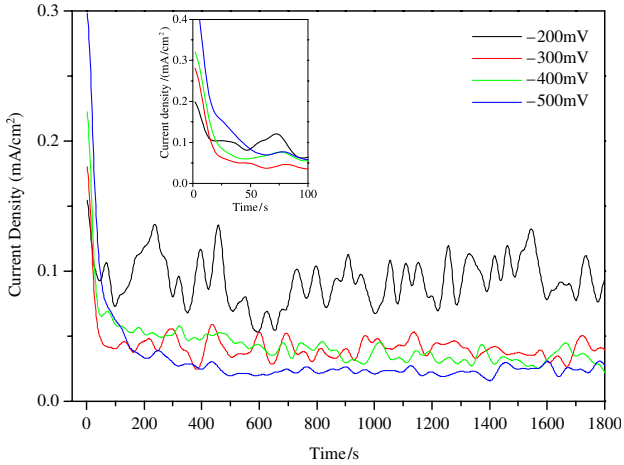

Fig. 2. Current density transients as a function of time for potentiostatic deposition at different potentials at room temperature in electrolytes consisting of 0.01*M* Cu^{2+} and 0.05*M* SCN^-. The inset shows a magnified view of the time range from 0 to 100 s.

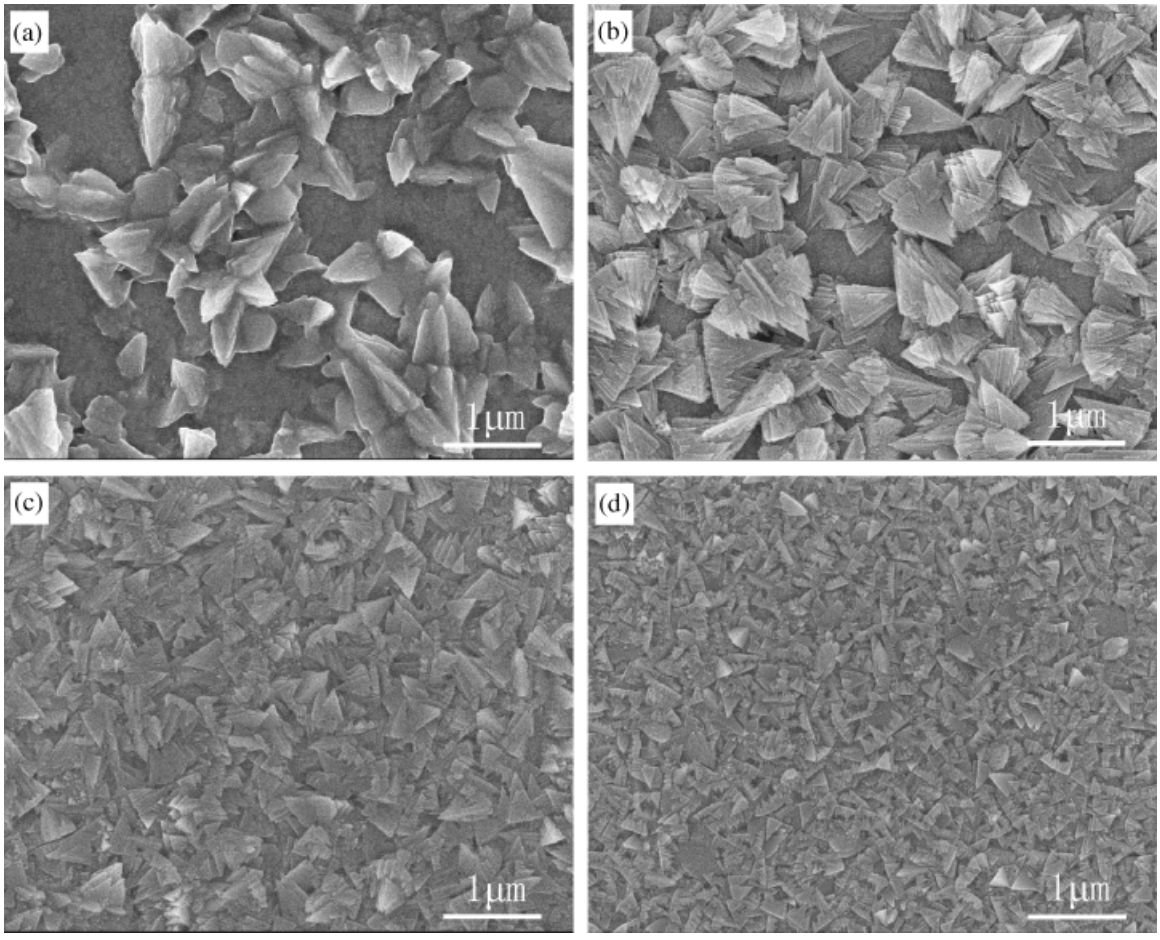

Fig. 3. Field-emission scanning electron microscopic images of the CuSCN films prepared in electrolytes consisting of 0.01*M* Cu^{2+} and 0.05*M* SCN^{-}, at different potentials: (a) −200 mV, (b) −300 mV, (c) −400 mV, (d) −500 mV, at room temperature.

and −500 mV to initiate the nucleation and growth. The recorded curves are shown in Fig. 2. In all transients, the rapid surge of current density at the onset of the potential was due to the double-layer charging, and then the current density decayed gradually because of an increase in the electric resistance of the electrochemical cell system, especially including the nucleation and growth of CuSCN crystals as semiconductor characteristics. In this current-decay stage, the magnitudes of the current density and the degradation were not the same for different applied potentials. A higher potential led to a larger current density and a slower degradation. Figure 3 shows the FESEM images of the resultant CuSCN films prepared during the chronoamperometry measurements. As shown in Fig. 3(a), when the applied potential was −200 mV, only sparse CuSCN grains could be seen on the surface of the ITO substrate due to the small amount of CuSCN nuclei formed on the ITO substrate at the low applied potential. The grain size grown at −200 mV was about 1 μm. When the potential increased to −300 mV, the relatively higher current density accelerated the nucleation and growth of CuSCN. As can be seen in Fig. 3(b), more CuSCN grains were formed on the ITO substrate, but the bare areas on the substrate were still present. The film grown at this potential had a smaller grain size (about 500 nm). At potentials of −400 and −500 mV, the surface of the ITO substrate was completely covered with well-grown CuSCN grains, and the grain size decreased to about 200 and 100 nm, respectively. Furthermore, compared with these images, the particle morphology was also different at different applied potentials. The sample grown at a lower potential (−200 mV) was not well grown, with some defects in the grain figure. With an increase in the potentials, the intrinsic morphology of a trigonal pyramid[34] appeared more obviously. The above-mentioned result indicates that the increased potential may lead to a high nucleation rate and more uniform nucleation on a large area and smaller grain size due to a high nuclei density. Hence, eventually a dense film with a fine grain size can be obtained at a potential as high as possible for sole deposition of CuSCN. This potential was −500 mV using the TEA-chelated aqueous electrolyte solution.

It can be observed from Fig. 2 that the current density transients plateau in the later stage, but still oscillate in the horizontal range. The plateau current density is defined as a saturated current density, which is determined by the electric resistance of the electrochemical cell.[35] Firstly, at different applied potentials, the consumption rates of the cations and anions in solutions were different so that the thickness of the diffusion layers in solutions differed. And secondly, from the FESEM observation, the distinct morphology of films deposited at different applied potentials led the layers of CuSCN obtained to attain different electric resistance. As a result, the saturated current density curves varied according to both main effects, where high electric resistance retained stable current density. In addition, the oscillation of the current density seems to be related to the rough surface morphology of the deposits. The electrodeposited surfaces did not appear to be smooth, and hence the oscillations or unstable behaviors of the current density could be seen. The current density transient curve at −500 mV had the lowest fluctuation as a vivid contrast against the one at −200 mV.

The stoichiometric proportions of the CuSCN films prepared in the electrolyte solutions with the molar ratios $[Cu^{2+}]$:$[SCN^{-}]$ of 1:10, 1:5, and 1:1 at potentiostatic −500 mV and room temperature were measured by XPS. The results are shown in Table I and Fig. 4, in which the content of S represents the SCN content in the film because S will not be imported as absorbed impurities from ambient. It can be seen from Table I, from Fig. 4(a), that the stoichiometric proportions of SCN/Cu in films were all above 1 whenever the molar ratios of electrolyte

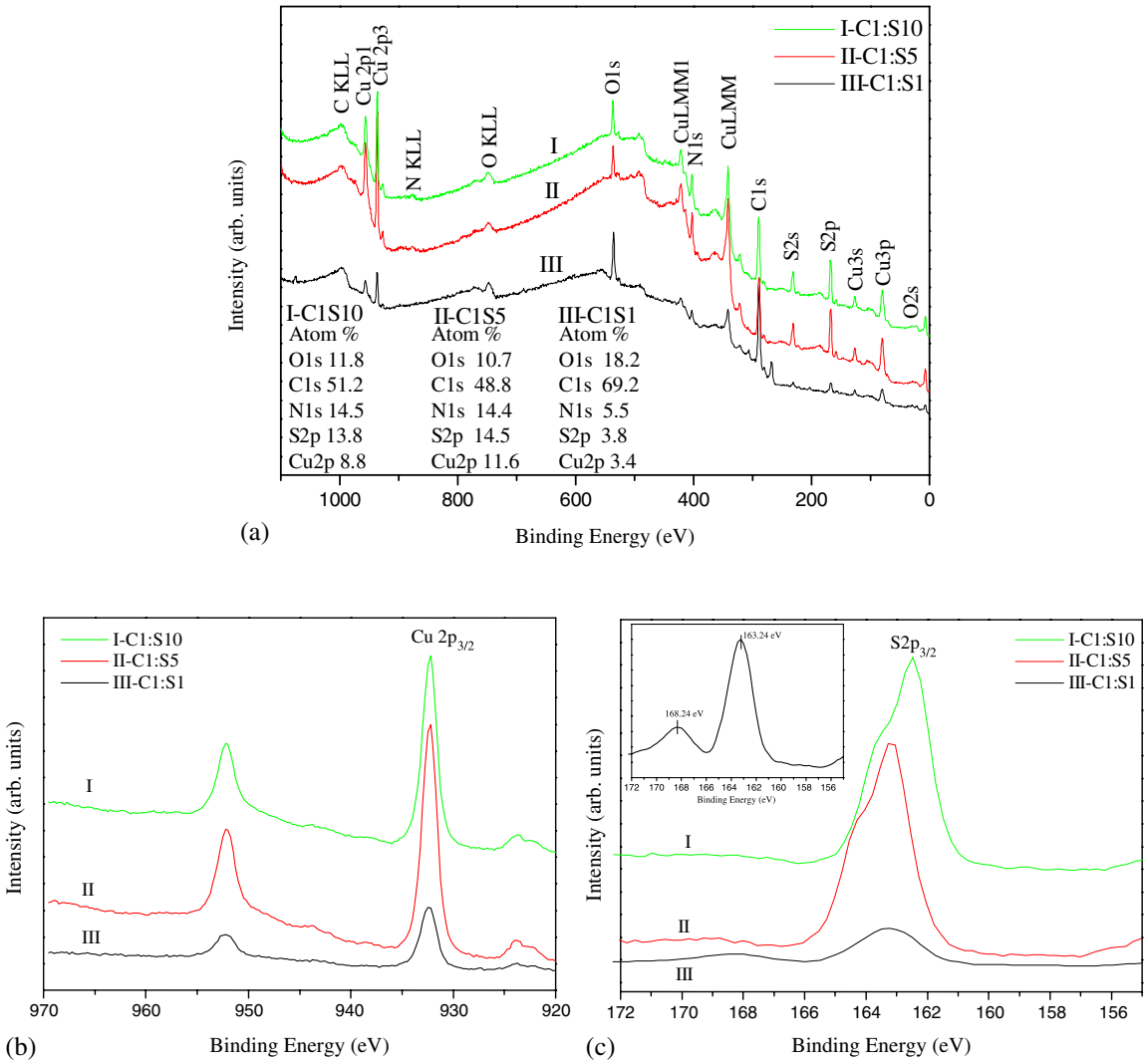

Fig. 4. X-ray photoelectron spectra (XPS) spectra of CuSCN films prepared from electrolyte solutions with different molar ratios $[Cu^{2+}]$:$[SCN^{-}]$ of 1:10, 1:5, and 1:1, at −500 mV and room temperature. (a) Full spectra, (b) Cu 2p core-level XPS spectra, (c) S 2p core-level XPS spectra. The inset shows the spectrum of the sample with molar ratio $[Cu^{2+}]$:$[SCN^{-}] = 1:1$. (C indicates Cu^{2+}, and S presents SCN^{-} in the electrolyte solutions; the followed numbers are molar ratios.)

solutions fluctuated. A higher molar ratio $[SCN^{-}]/[Cu^{2+}] = 10$ in the electrolyte solution led to a relatively higher stoichiometric proportion SCN/Cu = 1.57 in the film. Even though the molar ratio $[SCN^{-}]/[Cu^{2+}] = 1$, the stoichiometric proportion SCN/Cu still reached 1.12. In known reference, it was reported that when SCN was in stoichiometric excess, $Cu(SCN)_{1+x}$ would show *p*-type semiconductor characteristics.[36] However, verification is difficult in our experiments because the thin CuSCN films were electrodeposited on *n*-type ITO substrates only to form an ohmic contact, which disturbed the electrical measurements such as Hall measurements to determine the mobility type of the film. Despite this, we can still give an indirect evidence. Figure 5 gives a *I–V* characteristic of the junction between electrodeposited CuSCN and ZnO nanostructured layers. The junction clearly displays a nonlinear behavior, showing rectification. It is well known that ZnO is a natural *n*-type semiconductor and an *n–n* junction generally will not show a rectifying action. Hence, the result indicates that the CuSCN films electrodeposited in TEA-chelated aqueous solutions should be *p*-type, which is required for the application of NPC cells.

Table I. Stoichiometric Proportion of CuSCN Films from Different Electrolyte Solutions

Molar ratio $[SCN^{-}]/[Cu^{2+}]$ in electrolyte solutions	SCN/Cu in films
10	1.57
5	1.25
1	1.12

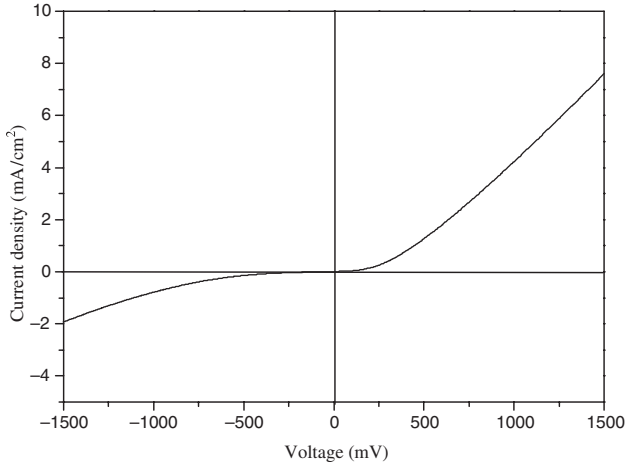

Fig. 5. Current–voltage (*I—V*) characteristic of the junction between CuSCN deposit and ZnO nanostructured layer.

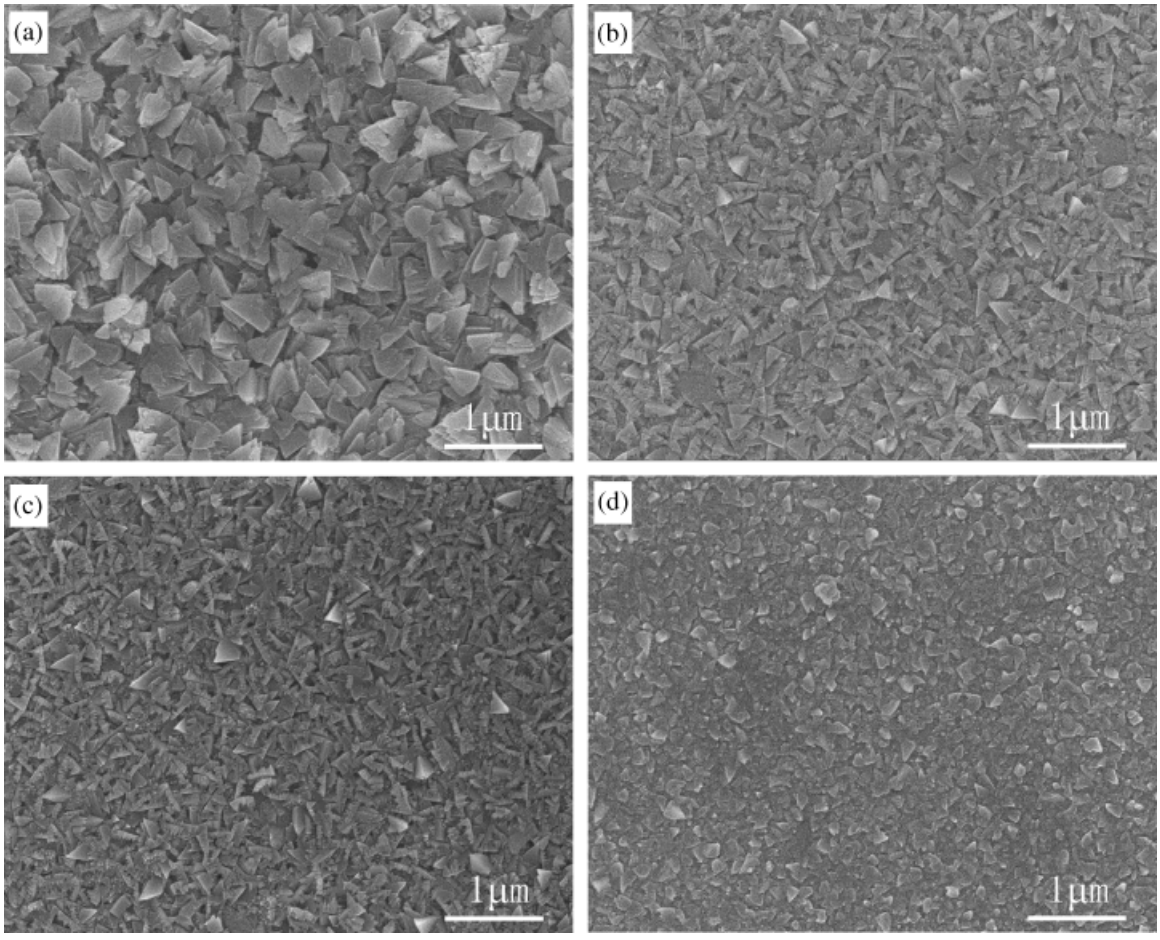

Fig. 6. Field-emission scanning electron microscopic images of the CuSCN films prepared with molar ratios $[Cu^{2+}]$:$[SCN^{-}]$ of (a) 1:10, (b) 1:5, (c) 1:3, and (d) 1:1, at –500 mV and room temperature.

Figure 4(b) shows the Cu 2p core level XPS spectra of the CuSCN films prepared at different molar ratios $[SCN^{-}]/[Cu^{2+}]$. The binding energy of Cu $2p_{3/2}$ is 932.24 eV when the molar ratio $[SCN^{-}]/[Cu^{2+}]$ is 10 or 5. But when the molar ratio $[SCN^{-}]/[Cu^{2+}]$ is 1, the binding energy of Cu $2p_{3/2}$ shifts to 932.49 eV. Both values are in good agreement with the values reported for CuSCN.[37] The shift of the binding energy may be attributed to a higher oxidation state of S existing in the film prepared at the molar ratio $[SCN^{-}]/[Cu^{2+}] = 1$. This is confirmed by the S 2p core-level XPS spectra shown in Fig. 4(c). The S $2p_{3/2}$ shows a main peak at 163.24 eV and a small shoulder at 168.24 eV, which is clearly shown in the inset. The main peak corresponds to S in SCN and the small shoulder may be due to S in SO_4^{2-} as one of the binding energy values of S $2p_{3/2}$ in SO_4^{2-} is 168.15 eV,[38] which is perhaps introduced from the use of $CuSO_4 \cdot 5H_2O$ as a raw material. However, at the molar ratios $[SCN^{-}]/[Cu^{2+}]$ of 10 or 5, such a small shoulder could not be found. In addition, it can be concluded that high atomic content of O and excess content of C are due to the absorption of O_2, CO_2 in air.

Figure 6 shows FESEM images of the CuSCN films derived from the electrolytes with molar ratios $[Cu^{2+}]$:$[SCN^{-}]$ of 1:10, 1:5, 1:3, and 1:1 at −500 mV and room temperature. It clearly shows that the intrinsic morphology of CuSCN is a trigonal pyramid. The growth with the molar ratio $[Cu^{2+}]$:$[SCN^{-}]$ of 1:10 showed random aggregates of trigonal pyramids (Fig. 6(a)). The smaller trigonal pyramid conjunct crystals with the same crystal orientation grew together at molar ratios $[Cu^{2+}]$:$[SCN^{-}]$ of 1:5 and 1:3 as shown in Figs. 6(b) and (c). When the molar ratio $[Cu^{2+}]$:$[SCN^{-}]$ decreased to 1:1, the defined trigonal pyramid could not be seen in Fig. 6(d). Combined with the XPS analysis, the grain not well-grown perhaps existed as SO_4^{2-} derived from the molar ratio $[Cu^{2+}]$:$[SCN^{-}]$ of 1:1, indicating that

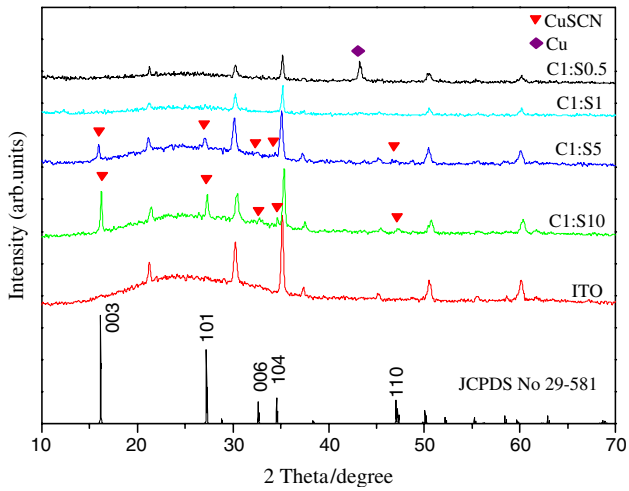

Fig. 7. X-ray diffraction (XRD) patterns of the CuSCN films prepared in different molar ratios $[Cu^{2+}]$:$[SCN^{-}]$ in electrolyte solutions, at −500 mV and room temperature. (C indicates Cu^{2+}, and S indicates SCN^{-}; the followed numbers are molar ratios.) The XRD pattern of bare indium tin oxide glass and the standard diffraction pattern of β-CuSCN (JCPDS card number 29-581) are also shown as references.

Fig. 10. Field-emission scanning electron microscopic images of the CuSCN films prepared at different temperatures: (a) 0°C, (b) 20°C, (c) 35°C, (d) 45°C, and (e) 55°C, in electrolytes consisting of 0.01*M* Cu^{2+} and 0.05*M* SCN^{-} at potentiostatic −500 mV.

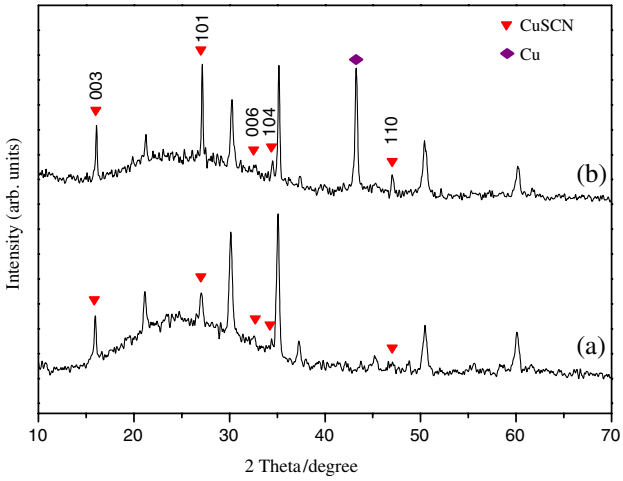

Fig. 8. X-ray diffraction patterns of the CuSCN films prepared at (a) room temperature and (b) 55°C, in the electrolyte consisting of 0.01*M* Cu^{2+} and 0.05*M* SCN^{-}, at −500 mV.

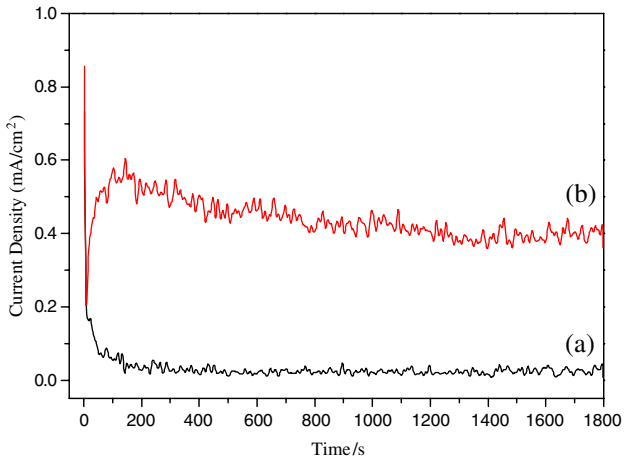

Fig. 9. Current density transients as a function of time for potentiostatic deposition at −500 mV at (a) room temperature and (b) 55°C in the electrolytes consisting of 0.01*M* Cu^{2+} and 0.05*M* SCN^{-}.

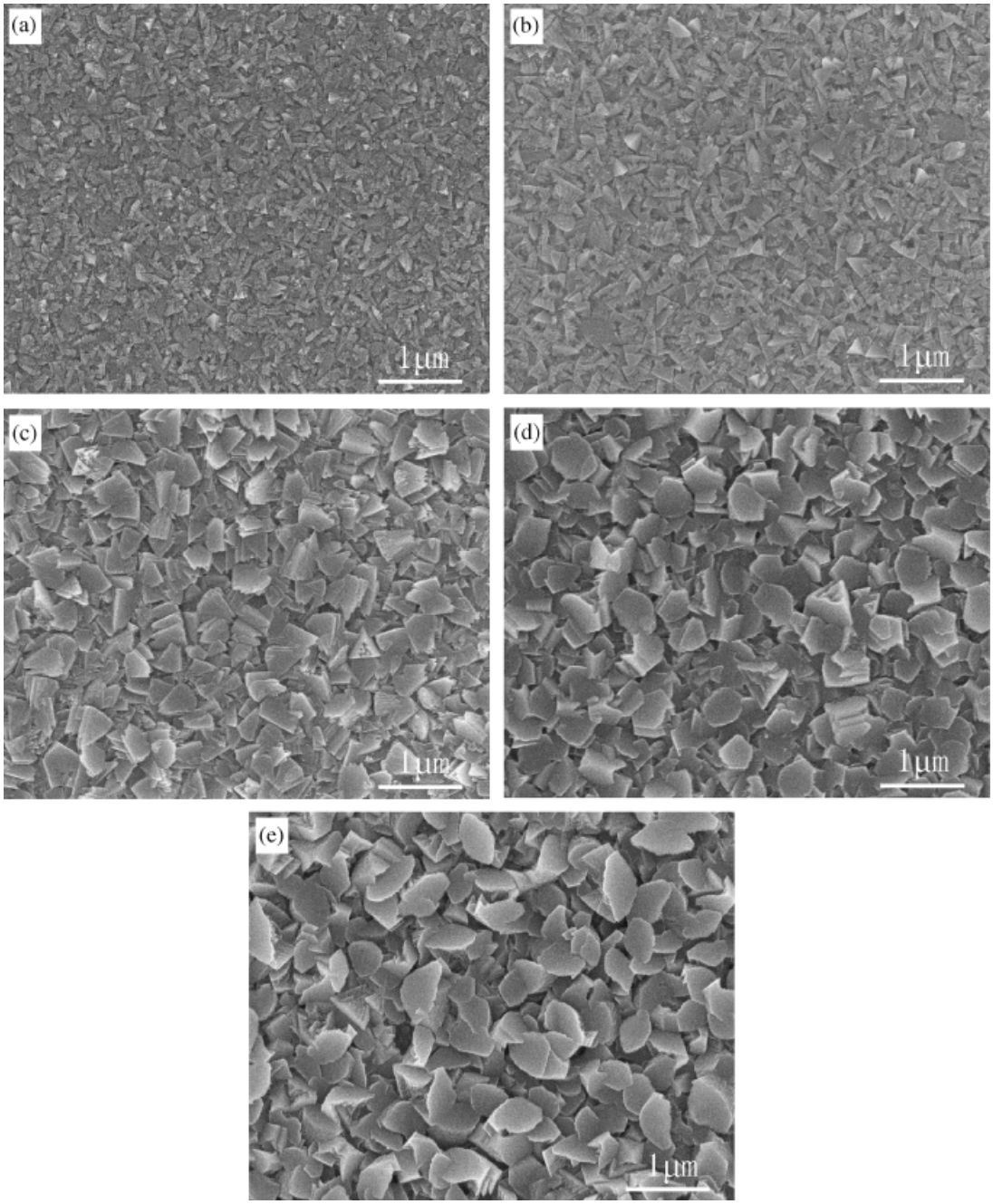

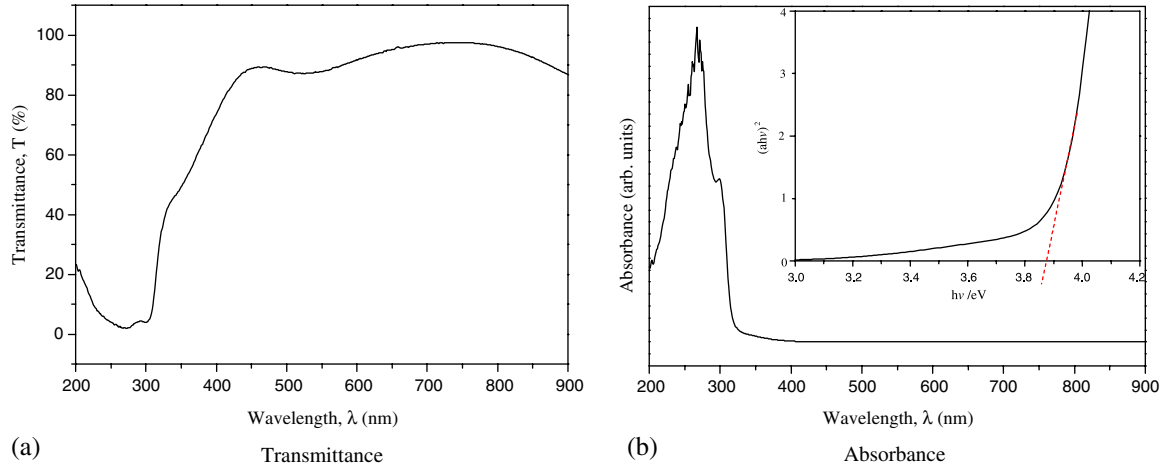

Fig. 11. Optical spectra of the CuSCN film prepared in the electrolyte consisting of 0.01*M* Cu^{2+} and 0.05M SCN^-, at potentiostatic −500 mV and room temperature. The inset shows the $(\alpha h\nu)^2$ versus $h\nu$ plot used for the determination of optical band gap of the CuSCN film.

this molar ratio was not an appropriate component of the electrolyte solution for CuSCN electrodeposition. Furthermore, it can be clearly concluded that the size of grains considerably decreases with a decline in the SCN^- concentrations in electrolyte solutions.

The XRD patterns of the CuSCN films electrodeposited with molar ratios $[Cu^{2+}]$:$[SCN^-]$ of 1:10, 1:5, 1:1, and 1:0.5 at −500 mV and room temperature are shown in Fig. 7, and that of the bare ITO substrate is also shown as a reference. It can be seen that when the molar ratio $[Cu^{2+}]$:$[SCN^-]$ is 1:10 or 1:5, all characteristic peaks of the electrodeposited films (C1:S10 and C1:S5) are well consistent with β-CuSCN (JCPDS card number 29-581), except those of the ITO-conducting layer. However, when the molar ratio $[Cu^{2+}]$:$[SCN^-]$ was 1:1 (C1:S1), it failed to yield diffraction peaks of CuSCN. With a further decrease in the concentration of SCN^- such as sample C1:S0.5, the diffraction peaks showed Cu co-deposition in the CuSCN films and no CuSCN characteristic peaks. This may be caused by the insufficiency of SCN^- ions in the electrolyte so that when Cu^{2+} ions are reduced to Cu^+, there are not enough SCN^- ions to react with Cu^+ to form CuSCN. Hence, the redundant Cu^+ ions continue to be reduced to Cu. In conclusion, an appropriate excess of SCN^- concentration in the electrolyte solution is necessary to avoid Cu co-deposition, the existence of SO_4^{2-}, and not well-grown grains.

The changes in XRD patterns and FESEM images of the CuSCN films with temperature are shown in Figs. 8 and 10, respectively. Other processing conditions were the electrolytes of 0.01*M* Cu^{2+} and 0.05*M* SCN^- and a potential of −500 mV. When the temperature was above 45°C, there were apparently some brown-colored points dispersed on the film surface, clearly indicating the co-deposition of Cu. The typical sample prepared at 55°C also shows the characteristic peak of copper in Fig. 8(b). It shows that Cu is easier to co-deposit at a higher temperature. Figure 9 shows the current density transients at room temperature and 55°C, and the curve of 55°C showed a metal copper deposition, clearly ascending in the early stage of the current density. The evolution of the morphology of the CuSCN films with the temperature shows that the grain size of CuSCN is enhanced with an increase in temperature. At a low temperature (0° and 20°C), the as-prepared films are small trigonal pyramid conjunct crystals, and the orientation of the conjunct crystals is random. When the temperature increased, the crystals grew like single trigonal pyramids. At temperatures of 45° and 55°C, the bottom of more single trigonal pyramids could be seen in the FESEM images, likely indicating preferred crystal orientation at an elevated temperature. The preferred orientation of CuSCN has also been reported in the upended taper-shaped CuSCN arrays prepared by a liquid–solid reaction between a copper substrate and an aqueous solution of NH_4CNS at room temperature.[39] From the XRD patterns in Fig. 8, it can be seen that the peak intensities of CuSCN at (003) and (101) planes at room temperature and 55°C are different. The relatively higher intensity of (101) plane at 55°C further provides information regarding the preferred orientation of the crystal along this plane.

The optical property of a typical CuSCN film with a film thickness of ~230 nm is shown in Fig. 11. The film was prepared in an electrolyte solution consisting of 0.01*M* Cu^{2+} and 0.05*M* SCN^-, at potentiostatic −500 mV and room temperature. The transmittance spectrum Fig. 11(a)) showed a high optical transmission value above 87% in the visible wavelength range. A significant increase in the absorption wavelength range lower than 320 nm can be assigned to the intrinsic band gap absorption of β-CuSCN. For direct band gap semiconductors, the absorption coefficient can be expressed as $\alpha h\nu = A(h\nu - E_g)^{1/2}$. According to the formula and the graph of $(\alpha h\nu)^2$ versus $h\nu$ as illustrated in the inset of Fig. 11(b), the optical band gap E_g of the typical CuSCN film equals to 3.88 eV. The band gap value is slightly higher, 0.28 eV, than that of the reported CuSCN films on a copper plate.[36] The crystal size of the sample measured optical band gap was estimated by the Debye–Scherrer formula; along the (003) peak, the size was ~21.8 nm while along the (101) peak it was ~18.2 nm. Hence, the blue shift of the band gap may be attributed to the stoichiometric excess of SCN in the electrodeposited film[31] and the trigonal pyramid conjunct crystals on a nanometer scale.

IV. Conclusions

A novel technique was developed to prepare a β-CuSCN film using a basic aqueous solution with TEA as a chelating agent. Mild electrolytes with pH values in the range of 8.5–9 were available for those deposition substrates that need to prevent acid etching such as with ZnO. Experimental results showed that the optimal electrodeposition potential was −500 mV for the sole CuSCN electrodeposition in the TEA-chelated aqueous solutions, and above it Cu would be co-deposited, and below it growth of CuSCN would be impaired. The electrodeposited films were hexagonal β-CuSCN with trigonal pyramid and stoichiometric excess of SCN by XRD and XPS characterization. The *I–V* characteristic of the junction between electrodeposited CuSCN and ZnO nanostructured layer indicated *p*-type semiconductor characteristics of the CuSCN films prepared. At the applied potential of −500 mV, the XPS spectrum of the film from the molar ratio $[Cu^{2+}]$:$[SCN^-]$ = 1:1 showed that SO_4^{2-} may be present. Cu co-deposition appears in the film with a molar ratio $[Cu^{2+}]$:$[SCN^-]$ = 1:0.5 due to the insufficiency of SCN^-. The grain size could be controlled by the component of electrolyte, and dense films with small trigonal pyramid conjunct crystals were achieved when the molar ratio $[Cu^{2+}]$:$[SCN^-]$ was 1:5 and 1:3. At deposition temperature ≥ 45°C, Cu could be co-deposited more easily, and the films obtained tended to have

a larger grain size and preferred orientation along with the (101) plane. The as-prepared CuSCN film had high transmittance $\geq 87\%$ in the visible wavelength range and its direct band gap was 3.88 eV.

Acknowledgments

The authors wish to acknowledge Fei He, Haiyan Du, Yuqing Duan, and Dongqing Jiang, for their kind assistance in the XPS, XRD, FESEM, and UV-Vis measurements, respectively.

References

[1]B. O'Regan and M. Grätzel, "A Low-Cost, High-Efficiency Solar Cell Based on Dye-Sensitized Colloidal TiO_2 Films," *Nature*, **353**, 737–40 (1991).

[2]U. Bach, D. Lupo, P. Comte, J. E. Moser, F. Weissörtel, J. Salbeck, H. Spreitzer, and M. Grätzel, "Solid-State Dye-Sensitized Mesoporous TiO_2 Solar Cells with High Photon-to-Electron Conversion Efficiencies," *Nature*, **395**, 583–5 (1998).

[3]K. Tennakone, G. R. R. A. Kumare, I. R. M. Kottegoda, K. G. U. Wijayantha, and V. P. S. Perera, "A Solid-State Photovoltaic Cell Sensitized with a Ruthenium Bipyridyl Complex," *J. Phys. D Appl. Phys.*, **31**, 1492–6 (1998).

[4]B. O'Regan and D. T. Schwartz, "Large Enhancement in Photocurrent Efficiency Caused by UV Illumination of the Dye-Sensitized Heterojunction TiO_2/RuLL'NCS/CuSCN: Initiation and Potential Mechanisms," *Chem. Mater.*, **10**, 1501–9 (1998).

[5]B. O'Regan, D. T. Schwartz, S. M. Zakeeruddin, and M. Grätzel, "Electrodeposited Nanocomposite *n–p* Heterojunctions for Solid-State Dye-Sensitized Photovoltaics," *Adv. Mater.*, **12** [17] 1263–7 (2000).

[6]V. P. S. Perera, P. K. D. D. P. Pitigala, P. V. V. Jayaweera, K. M. P. Bandaranayake, and K. Tennakone, "Dye-Sensitized Solid-State Photovoltaic Cells Based on Dye Multilayer-Semiconductor Nanostructures," *J. Phys. Chem. B*, **107**, 13758–61 (2003).

[7]K. Peter, H. Wietasch, B. Peng, and M. Thelakkat, "Dual-Functional Materials for Interface Modifications in Solid-State Dye-Sensitised TiO_2 Solar Cells," *Appl. Phys. A Mater.*, **79**, 65–71 (2004).

[8]C. Lévy-Clément, R. Tena-Zaera, M. A. Ryan, A. Katty, and G. Hodes, "CdSe-Sensitized *p*-CuSCN/Nanowire *n*-ZnO Heterojunctions," *Adv. Mater.*, **17** [12] 1512–5 (2005).

[9]A. Wahi and R. Könenkamp, *Proceedings of the 11th Photovoltaic Solar Energy Conference, Montreux, Switzerland, 1992*, p. 714. Harvard Academic Publishers, Cambridge, MA, 1993.

[10]*Proceedings of 16th Europen Photovoltaic Solar Energy Conference, Glasgow, U.K., May 1–5*, Edited by H. Scheer, B. McNelis, W. Palz, H. A. Ossenbrink, and P. Helm, James and James, London, 2000.

[11]C. Lévy-Clément, A. Katty, S. Bastide, F. Zenia, I. Mora, and V. Munoz-Sanjose, "A New CdTe/ZnO Columnar Composite Film for Eta-Solar Cells," *Phys. E*, **14**, 229–32 (2002).

[12]K. Ernst, A. Belaidi, and R. Könenkamp, "Solar Cell with Extremely Thin Absorber on Highly Structured Substrate," *Semicond. Sci. Technol.*, **18**, 475–9 (2003).

[13]R. Tena-Zaera, A. Katty, S. Bastide, C. Lévy-Clément, B. O'Regan, and V. Munoz-Sanjose, "ZnO/CdTe/CuSCN, a Promising Heterostructure to Act as Inorganic Eta-Solar Cell," *Thin Solid Films*, **483**, 372–7 (2005).

[14]R. Tena-Zaera, M. A. Ryan, A. Katty, G. Hodes, S. Bastide, and C. Lévy-Clément, "Fabrication and Characterization of ZnO Nanowires/CdSe/CuSCN Eta-Solar Cell," *C. R. Chim.*, **9**, 717–29 (2006).

[15]R. Könenkamp, K. Ernst, Ch.-H. Fischer, M. C. Lux-Steiner, and C. Rost, "Semiconductor Growth and Junction Formation within Nano-Porous Oxides," *Phys. Stat. Sol. (a)*, **182**, 151–5 (2000).

[16]K. Tennakone, V. P. S. Perera, I. R. M. Kottegoda, and G. R. R. A. Kumare, "Dye-Sensitized Solid State Photovoltaic Cell Based on Composite Zinc Oxide/Tin (IV) Oxide Films," *J. Phys. D Appl. Phys.*, **32**, 374–9 (1999).

[17]W. C. Sinke and M. M. Wienk, "Photochemistry: Solid-State Organic Solar Cells," *Nature*, **395**, 544–5 (1998).

[18]B. Li, L. D. Wang, B. Kang, P. Wang, and Y. Qiu, "Review of Recent Progress in Solid-State Dye-Sensitized Solar Cells," *Sol. Energy Mater. Sol. Cells*, **90**, 549–73 (2006).

[19]B. O'Regan and D. T. Schwartz, "Efficient Photo-Hole Injection from Adsorbed Cyanine Dyes into Electrodeposited Copper(I) Thiocyanate Thin Films," *Chem. Mater.*, **7**, 1349–54 (1995).

[20]K. Tennakone, G. R. R. A. Kumara, A. R. Kumarasinghe, K. G. U. Wijayantha, and P. M. Sirimanne, "A Dye-Sensitized Nano-Porous Solid-State Photovoltaic Cell," *Semicond. Sci. Technol.*, **10**, 1689–93 (1995).

[21]K. Murakoshi, R. Kogure, and S. Yanagida, "Solid State Dye-Sensitized TiO_2 Solar Cell With Polypyrrole as Hole Transport Layer," *Chem. Lett.*, **5**, 471–2 (1997).

[22]J. Krüger, R. Plass, L. Cevey, M. Piccirelli, and M. Grätzel, "High Efficiency Solid-State Photovoltaic Device Due to Inhibition of Interface Charge Recombination," *Appl. Phys. Lett.*, **79** [13] 2085–7 (2001).

[23]H. Kawazoe, M. Yasukawa, H. Hyodo, M. Kurita, H. Yanagi, and H. Hosono, "P-Type Electrical Conduction in Transparent Thin Films of $CuAlO_2$," *Nature*, **389**, 939–42 (1997).

[24]J. J. He, H. Lindström, A. Hagfeldt, and S. E. Lindquist, "Dye-Sensitized Nanostructured *p*-Type Nickel Oxide Film as a Photocathode for a Solar Cell," *J. Phys. Chem. B*, **103**, 8940–3 (1999).

[25]K. Tennakone, A. R. Kumarasinghe, P. M. Sirmanne, and G. R. R. A. Kumare, "Deposition of Thin Polycrystalline Films of Cuprous Thiocyanate on Conducting Glass and Photoelectrochemical Dye-Sensitization," *Thin Solid Films*, **261**, 307–10 (1995).

[26]G. R. R. A. Kumara, A. Konno, G. K. R. Senadeera, P. V. V. Jayaweera, D. B. R. A. De Silva, and K. Tennakone, "Dye-Sensitized Solar Cell With the Hole Collector *p*-CuSCN Deposited from a Solution in *n*-Propyl Sulphide," *Sol. Energy Mater. Sol. Cells*, **69**, 195–9 (2001).

[27]B. R. Sankapal, E. Goncalves, A. Ennaoui, and M. Ch.Lux-Steiner, "Wide Band Gap *p*-Type Windows by CBD and SILAR Methods," *Thin Solid Films*, **451–452**, 128–32 (2004).

[28]D. C. Look, D. C. Reynolds, J. R. Sizelove, R. L. Jones, C. W. Litton, G. Cantwell, and W. C. Harsch, "Electrical Properties of Bulk ZnO," *Solid State Commun.*, **105**, 399–401 (1998).

[29]L. Forro, O. Chauvet, D. Emin, L. Zuppiroli, H. Berger, and F. Lévy, "High mobility *n*-type Charge Carriers in Large Single Crystals of Anatase (TiO_2)," *J. Appl. Phys.*, **75**, 633–5 (1994).

[30]B. O'Regan and D. T. Schwartz, "Efficient Dye-Sensitized Charge Separation in a Wide-Band-Gap *p–n* Heterojunction," *J. Appl. Phys.*, **80** [8] 4749–54 (1996).

[31]W. B. Wu, Z. G. Jin, Z. Hua, Y. N. Fu, and J. J. Qiu, "Growth Mechanisms of CuSCN Films Electrodeposited on ITO in EDTA-Chelated Copper(II) and KSCN Aqueous Solution," *Electrochim. Acta.*, **50**, 2343–9 (2005).

[32]A. J. Bard and L. R. Faulkner, *Electrochemical Methods Fundamentals and Applications (Chapter 5)*, 2nd edition, John Wiley & Sons Inc., New York, 2003.

[33]J. A. Switzer, C. J. Huang, E. W. Bohannan, M. G. Shumsky, T. D. Golden, and D. C. Van Aken, "Electrodeposition of Quantum-Confined Metal/Semiconductor Nanocomposites," *Adv. Mater.*, **9** [4] 334–8 (1997).

[34]D. L. Smith and V. I. Saunders, "The Structure and Polytypism of the β Modification of Copper(I) Thiocyanate," *Acta Cryst. B*, **37**, 1807–12 (1981).

[35]M. Saitou and Y. Fukuoka, "An Experimental Study on Stripe Pattern Formation of Ag–Sb Electrodeposits," *J. Phys. Chem. B*, **108**, 5380–5 (2004).

[36]K. Tennakone, A. H. Jayatissa, C. A. N. Fernando, S. Wickramanayake, S. Punchihewa, L. K. Weerasena, and W. D. R. Premasiri, "Semiconducting and Photoelectrochemical Properties of *n*- and *p*-Type β-CuCNS," *Phys. Stat. Sol. (a)*, **103**, 491–7 (1987).

[37]M. Yang, J. J. Zhu, and J. J. Li, "Synthesis and Characterizations of Porous Spherical CuSCN Nanoparticles," *Mater. Lett.*, **59** [7] 842–5 (2005).

[38]X. R. Yu, F. Liu, Z. Y. Wang, and Y. Chen, "Auger Parameters for Sulfur-Containing Compounds Using a Mixed Aluminum–Silver Excitation Source," *J. Electron Spectrosc. Relat. Phenom.*, **50**, 159–66 (1990).

[39]J. S. Xu and D. F. Xue, "Fabrication of Upended Taper-Shaped Cuprous Thiocyanate Arrays on a Copper Surface at Room Temperature," *J. Phys. Chem. B*, **110**, 11232–6. □